Journal of Applied Engineering and Technological Science
Vol 7(2) 2026: 1253-1273

HUMAN BRAIN TUMORS DETECTED BY A DEEP LEARNING METHOD THROUGH A PRE-TRAINED MODEL

Hanan H. Al-Nidawi[1], Farah K. AL-Jibory[2*], Mohammed S. Hamid[3], Ruaa S. Salman[4]
Ministry of Education, General Directorate of Administrative Affairs, Baghdad, Iraq[1]
Ministry of Education, Karkh First Directorate of Education, Baghdad, Iraq[2]
Ministry of Education, Baghdad, Iraq[3]
Ministry of Education, Karkh Three Directorate of Education, Baghdad, Iraq[4]
hananhazem654@gmail.com[1], csd1b0037@gmail.com[2*], m.hamidnth@gmail.com[3],
ruaa.s.alkhafaji@gmail.com[4]

Received: 07 November 2025, Revised: 19 April 2026, Accepted: 22 April 2026
**Corresponding Author*

ABSTRACT
As a result, abnormal cells develop in the body, leading to a highly constitutive cell type that is a significant risk to the patient's functional capabilities and vital processes. The early and accurate recognition of such cells is crucial for accurate diagnosis and prognosis, and this recognition is made possible by medical imaging techniques, particularly magnetic resonance imaging (MRI). Despite advances in 3D learning models, several scientific studies involving deep convolutional networks (CNNs) still face numerous challenges. These challenges include the underutilization of spatial information, the inability of traditional data reduction techniques to minimise data dimensionality during the assembly phase, and suboptimal data processing during the data synchronisation or listening. In addition, some approaches require large volumes of data to achieve sufficient performance, which limits their applicability to real-world healthcare scenarios. This paper discusses the V-Net model that has been trained for a relatively long time to process volumetric 3D data, including a wide variety of very small sub-3D spatial volumes. This work used a large global MRI dataset, split into 80% for the training set and 20% for the test set. Before the tests, the images were preprocessed by resizing them to 128 × 128, applying Min-Max normalisation, and CLAHE (Contrast Limited Adaptive Histogram Equalisation) to enhance contrastof the images. The results showed that the proposed model achieved a 99% improvement in tumour detection performance over all other approaches. The findings indicate that employing specialised architectures like V-Net may significantly enhance the efficiency of medical diagnostic imaging specialists.

Keywords: *Brain, Tumour, MRI, Deep Learning, Detection.*

1. Introduction

Brain tumours are dangerous medical illnesses and are associated with increased mortality. They stem from abnormal growth of neural tissue, which directly affects the functioning of the nervous system and nearby organs. Depending on its location, volume, and rate of expansion, the tumour can cause profound cognitive and functional deficits (Soomro et al., 2022). There are two main types of brain tumours: primary tumours, which arise from the brain, and secondary (metastatic) tumours, which originate from other parts of the body and spread to the brain (Jia & Chen, 2020). They may be categorised as benign or malignant (cancerous), with their effects differing based on their biological attributes and anatomical position within the brain (B. Chen et al., 2021). Over the past few years, MRI technology has become increasingly important for detecting brain tumours. This is due to MRI's unmatched ability to differentiate and visualise various tissue characteristics. In addition, the ongoing advances in deep learning have spurred the development of numerous models to simplify the analysis of brain imaging data. For instance, U-Net has proven highly effective for medical image segmentation. In contrast, those models facilitate image classification. Recently, medical imaging has also benefited from the use of Vision Transformers, owing to their superior ability to analyse and interpret complex details in images. (Hu & Razmjooy, 2021). Notwithstanding this advancement, considerable obstacles persist. The primary limitations include the inadequate capacity of certain conventional 2D models to represent 3D spatial data and the degradation of intricate details during the process of dimensionality reduction (Tiwari et al., 2020). Moreover, the assessment of many advanced models, including V-Net, remains confined to general and varied datasets, hence constraining the applicability of their findings in practical scenarios. Furthermore, numerous research has concentrated exclusively on classification tasks, neglecting the exact delineation of tumour boundaries(Sanjay & Swarnalatha, 2022).

The gap in the research lies in the need to have a model that can accurately segment brain tumours using 3D MRI data, determine its effectiveness on general data, and compare the results of segmentation to a final diagnosis (affected/unaffected). This article promotes the use of a 3D V-Net model to accurately segment brain tumours, taking advantage of its ability to process volumetric data and extract contextual information of different segments. The innovation in this work is the combination of accuracy of segmentation with results to aid the classification process, thereby enhancing diagnostic accuracy and relevance of the system in real-world medical settings. Also, the preliminary data processing is done to ensure quality in the input stage of training process.

2. Literature Review

Brain tumors are a very serious disease that has very high mortality rate and early diagnosis is very crucial to enhancing the treatment and survival of the patients. Artificial intelligence (AI) has become a potent resource of early tumor detection over the last few years and became a focal point of research in the given field. Nevertheless, there are still a number of difficulties concerning the development of efficient diagnostic systems. It is still challenging to detect very small tumors especially those that are smaller than 3 mm. Also, most of the current methods handle medical images not as sequential data but as a collection of images, thereby constraining the capacity of neural networks to learn spatial continuity across slices. The other big problem is the inability to determine the types of tumors using MRI since the MRI data usually includes several views-axial, coronal and sagittal which generate a series of images as one passes through the outer to the inner cortex. These complications underscore the fact that there is a need to have sophisticated methods that are able to process multi-view and multi-slice data in real time. To this end, the proposed system will focus on overcoming these limitations by creating a neural network that will handle the three MRI parts in a unified manner, sequence of images instead of individual images, and classify the type, location and size of the tumor. This is also supported by an application that has user friendly and interactive interfaces to enable easy and effective use of the proposed approach.

The Challenge in Brain Tumor can be divided into two aspects where the first is medical, and the second is applied:

a) Medical

Treatment for brain tumors has been complex, primarily because of the molecular features of these diseases, which frequently work together to impede healing. Initially, by entering one of the essential organs in the body, Even the most experienced neurosurgeons frequently cannot access these tumors because of their location (Sampson et al., 2020). These tumors are also situated behind the blood-brain barrier (BBB), a network of transport proteins and tight junctions that shield vulnerable brain regions from the elements present in the bloodstream, preventing systemic chemotherapeutic exposure. Moreover, these tumors are often resistant to both traditional and cutting-edge therapies due to the distinct developmental, genetic, epigenetic, and micro-environmental characteristics of the brain. The fact that brain tumors are more uncommon than many other types of cancer exacerbate these difficulties; this draws a small and dispersed research group and restricts the amount of financing and interest from the pharmaceutical sector (Arvanitis et al., 2020).

b) Applied

It is difficult to diagnose brain tumors with artificial intelligence. This section addresses unresolved problems and tasks that have been covered in the literature:

The Variations in Datasets A multitude of datasets are accessible for the diagnosis of brain tumors. Several datasets are available to the public, while others are not available to the general public. Different datasets use different image dimensions(Chahal et al., 2020).

Number of Images in Dataset is Researchers gathered images from patients in various hospitals to create a dataset. Because there are different numbers of low-grade and high-grade tumors in each dataset, there are differences in the number of images in each dataset (Tchoketch Kebir et al., 2019). The Tumor Size is the size of the tumor matters. If the lesion is less than 3 mm in size, it is challenging to identify the tumor (Gordillo et al., 2013). The Patients' Age is It was noted in the literature that every single patient's data is gathered from individuals whose ages range from 40 to 70 on average. However, no information was gathered from younger patients (Chahal et al., 2020). Skull base tumor types comprise is the term "skull base tumor" describes the tumor's location. However, not all skull base tumors are created equal. Tumors can be of several types. Additionally, the fact that each form of skull base tumor grows differently must be considered when receiving treatment(Arabahmadi et al., 2022)(Singh, 2016) .

⇒ Acoustic Neuromas

Vestibular schwannoma, another name for acoustic neuroma, is a benign (noncancerous) tumor. It originates in the cells encircle the hearing and balance nerve, which links your brain and ears. The majority of auditory neuromas grow exceptionally slowly. At the same time, the tumors start to press against the surface of the brain stem, the cerebellum, and adjacent blood vessels (the base of the brain). The pressure from a developing acoustic neuroma brings on the symptoms. Over 5,000 individuals in the U.S. are given an acoustic neuroma diagnosis each year. They are often between the ages of 30 and 60(Neugut et al., 2019). Each acoustic neuroma case was measured from the right side to the left side (Rt. to Lt.), the anterior side to the posterior side (A.P.), and the cephalic side to the caudal side (C.C.). The most significant measurements were taken for each acoustic neuroma tumor. A simple Excel analysis of the mean in every category analyzed the measurements. Each acoustic neuroma case was given a Koos score based on the MRI scan's measurements and findings(Alahmari, 2020). See Figure. 1

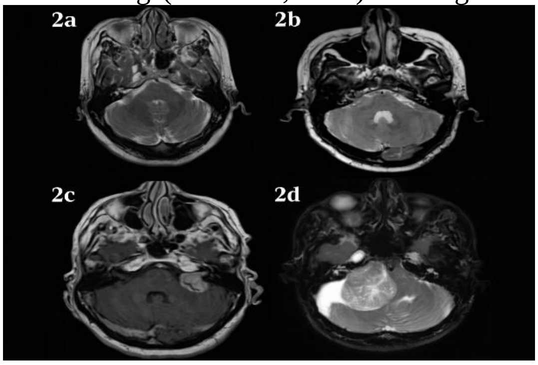

Fig. 1. Koos' Grading System for Acoustic Neuroma. The (1a) Is Grade 1, An Intracanalicular Tumor, (1b) Is Grade 2, A Cerebellopontine Angle Tumor with Minimal Extension <(2 Cm, (1c) Is A Grade 3, A Cerebellopontine Angle Tumor with No Cerebellar Trunk Displacement <3 Cm, And (1d) Is Grade 4, A Massive Tumor That Displaces The Brainstem >3 Cm(Alahmari, 2020).

⇒ Craniopharyngiomas

A benign growth near the base of the brain called a craniopharyngioma, does not indicate that cancer is usually located above the pituitary. These tumors' precise cause is unknown. The majority of cases of craniopharyngiomas are diagnosed in adults over 50 and children under 15. The incidence is the same regardless of race or gender(Zhang et al., 2020). Segmentation of tumors Figure 2 displayed the tumor segmentation results with eight axial T1-MPRAGE MR images from a single BRAF mutant instance. The tumor was indicated by the red line surrounding the area in each photograph(X. Chen et al., 2019).

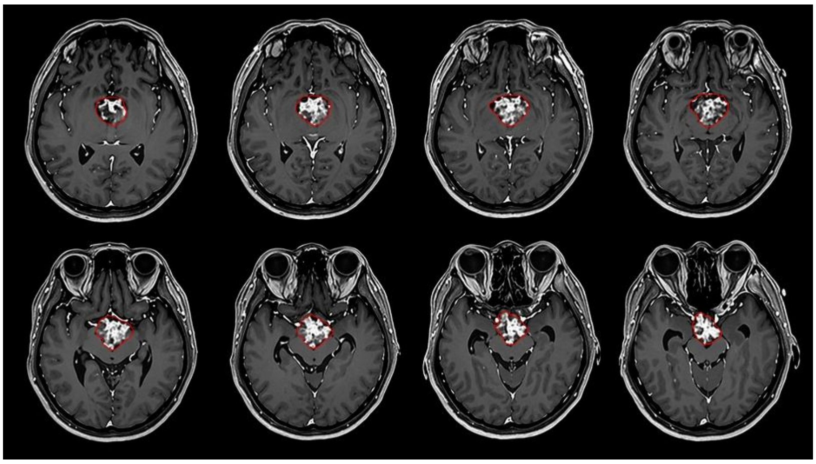

Fig. 2. Results of Tumour Segmentation from One BRAF Mutant Case Using Eight Representative Axial T1-PRAGE MR Images. The tumour is indicated in each image by the area surrounded by a red line. (X. Chen et al., 2019).

⇒ **Chordomas**

A slow-growing cancer of the spine tissue is called a chordoma. Chordomas can occur at any point in the spinal column. It is frequently seen either close to the tailbone (called sacral tumours) or at the junction of the spine and skull (called clival tumours). Another name for chordoma is notochordal sarcoma. (Mark et al., 2022). As seen in Figure 3, the brainstem, major arteries, and multiple cranial nerves are among the nearby features that make achieving this goal more challenging at the base of the skull. Clival chordoma is more common than upper spinal chordoma, with the former occasionally affecting the C1-2 level (Figure 3C) [19].

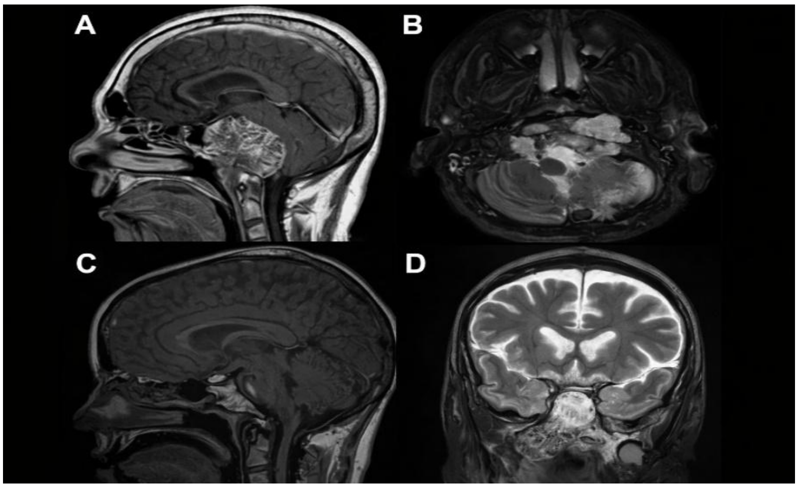

Fig. 3. Chordomas of The Base of The Skull Can Invade Different Anatomical Compartments. A Gadolinium-Enhanced MRI Sagittal T1 Reveals a Large Chordoma, Mostly Containing the Upper and Lower Clivuses. B Tumor Squeezing the Brain Stem and Infiltrating the Occipital Condyles Is Visible on The MRI Axial T2 Scan. C MRI Sagittal T2; The Tumor Is Encroaching on C2 And Other Lower Craniocervical Junction Compartments. D MRI Coronal T2: Massive Tumor Encroaching on Extracranial Spaces(Shimony et al., 2017).

⇒ **Chondrosarcoma**

An uncommon kind of cancer called chondrosarcoma typically starts in the bones, but it can also occasionally appear in the soft tissue next to bones. Most typically, chondrosarcoma affects the hip, shoulder, and pelvis. Less frequently, it may occur in the bones of the spine. (Deckers et al., 2020). The creation of a cartilage matrix by tumour cells unites the diverse group of neoplasms known as chondrosarcomas. (Gazendam et al., 2023). Following myeloma and osteosarcoma, chondrosarcoma is the third most frequent primary cancer of bone. After appropriate surgery, most of these tumours have an excellent prognosis because they rarely spread and grow slowly. (Gelderblom et al., 2008). To rule out a primary or metastatic malignant brain tumour, tomography was used (Figure 4a). Bria's magnetic resonance imaging (M.R.) was used to find an oval extra-axial mass (2.2 1.0 2.0 cm) in the interhemispheric fissure attached to the left surface of the falx cerebri. According to M.R. imaging, the lesion was hyperintense on T2-weighted images (Figure 4c) and iso-intense with the grey matter on T1-weighted images (Figure 4b) following gadolinium injection.(Tosaka et al., 2005).

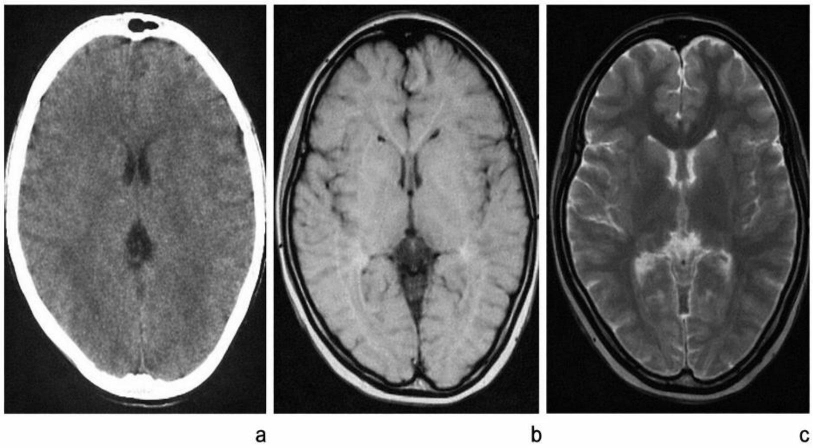

Fig.4. Chondrosarcoma Neuroimaging Was Incidentally Found Two Years Before Surgery. (A) C.T.'S Image Shows Many Tiny Intralesional Calcifications and A Small, Thick Lesion in The Left Area. (B) A Well-Enhanced Oval Extra-Axial Mass (2.2* 10* 2.0 Cm) in the Interhemispheric Fissure Connected to the Left Surface of the falx cerebri is visible on the T1-Weighted MR Image with Gadolinium. (C) T2-Weighted MR Image Demonstrating The Hyperintense Lesion With Comparatively Hypo-Intense Surrounding Tissue And No Perifocal Oedema (Tosaka et al., 2005).

⇒ **Meningiomas**

The meninges, also known as the Dura Mater, Arachnoid Mater, and Pia Mater, are three layers of membranes that surround the brain and spinal cord and protect them. A meningioma is a tumour that develops in the meninges.(David, 2019). A meningioma is a noncancerous (benign), slow-growing tumour that develops inside the skull, within the membranes that encircle the brain. So people with meningioma tumours often don't realise they have a brain tumour. (Georgiadis et al., 2011). People with a first-degree (benign) meningioma usually undergo surgery and radiation therapy. The tumour is likely to come back (recur) if it is not eliminated. Suppose it has not been eliminated. (Arokia Jesu Prabhu & Jayachandran, 2018). Meningiomas can take many forms, depending on where they occur. Meningiomas of the convex shape, flatulent shape, para-meningeal shape, intraventricular shape, meningioma at the base of the skull, sphenoid flank meningioma, olfactory groove meningioma, petroglyph meningioma, and recurrent meningioma are among them.(David, 2019). Examples of images of meningioma growth are shown in Figure 5, with tumours highlighted in red.(Rane, 2023).

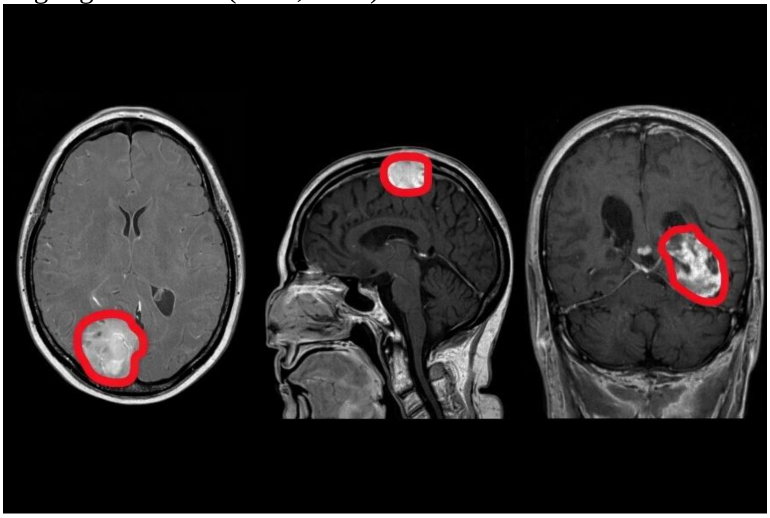

Fig. 5. MRI images of brain tumours as examples of meningioma type(Rane, 2023).

Every image depicts the growth of a meningioma tumour. Meningioma's axial cross-section is on the far left, its sagittal portion is in the middle, and its coronal section is on the far right. To make this figure work, the tumour masses were manually marked in red.

⇒ Paranasal Sinus Cancers (No)

Tumours are formed when cells in and around the nose grow and multiply abnormally, causing diseases known as nasal cavity and sinus cancers. (Harris et al., 2022). They could exhibit signs such as headaches or nasal congestion. While treating your sinus infection, your doctor might find the tumour. Cancers of the nose and sinuses are uncommon. (Cabezas-Camarero & Pérez-Segura, 2022). Only roughly 2,000 Americans are impacted by them annually. Most tumours in the sinuses or nasal cavities are benign, but some are malignant. Some tumour types that are not cancerous initially may develop into cancer if treatment is not received. You can feel more prepared to discuss your care and potential treatment options with your doctor if you know as much as you can about your diagnosis. If you or a loved one has received a diagnosis of sinus or nasal cancer, there are some details to get you going. (Taylor & Saba, 2021). In Figure 6, MRI is invaluable for summarising several patterns of localised expansion in sinus carcinomas.(Ferrari et al., 2021).

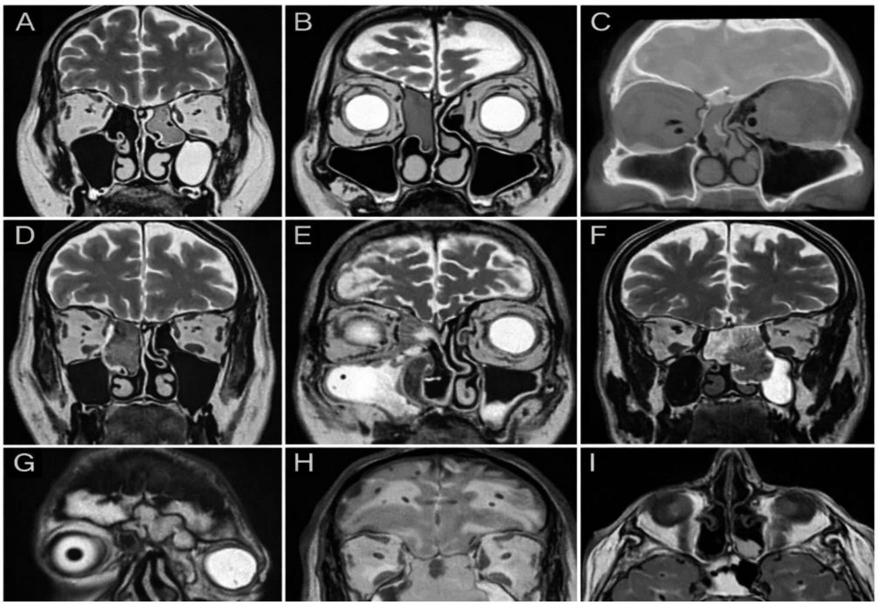

Fig. 6. Several Patterns of Loco-Regional Expansion Of MRI-Scanned Sinus Carcinomas Are Summarised (Ferrari et al., 2021).

⇒ Pituitary Adenomas

A pituitary tumour is an abnormal development in the pituitary gland. The pituitary is a small gland located in the brain. It is located behind the back of the nose and generates hormones that affect many other glands and functions. However, they may lead to an excess or insufficient production of hormones by the pituitary, which could result in health issues(Raverot & Ilie, 2022). The most prevalent type of tumour in the pituitary gland is a pituitary adenoma. "Adenoma" describes a benign tumour that starts in gland tissue. Although these incidents are rare, pituitary adenomas can develop into pituitary carcinomas. (Lake et al., 2013). In Figure 7, magnetic resonance imaging revealed a pituitary gland mass in two cases (Hashemzehi et al., 2020).

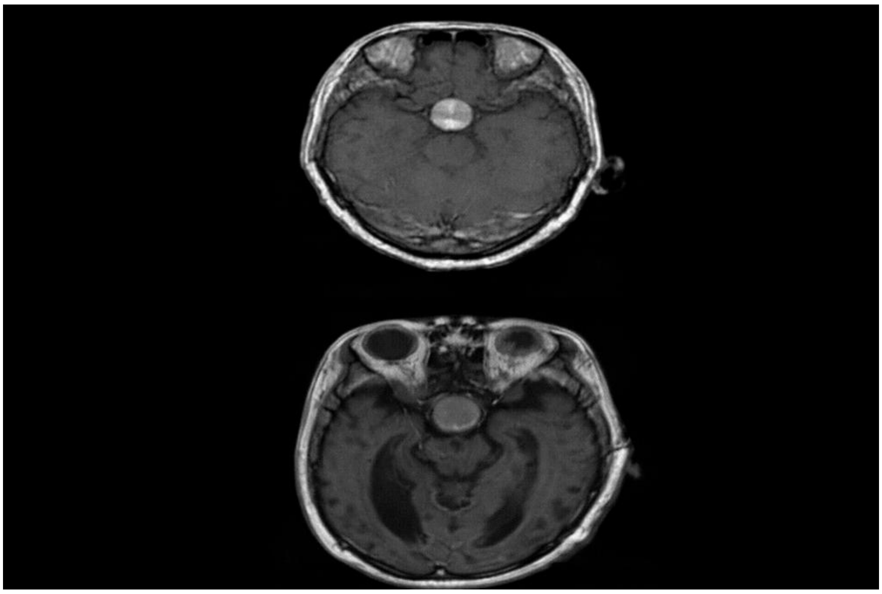

Fig. 7.Brain Tumour MRI Images (Pituitary Tumour) (Hashemzehi et al., 2020).

Adenomas can also develop outside of the pituitary gland in other parts of the body, encompassing the adrenal glands and the colon. These tumours are diagnosed by medical professionals based on their size and the hormones they secrete. Pituitary adenomas are classified into microadenomas (<10mm), macroadenomas (>=10 mm), and giant adenomas (>=40 mm), as shown in Figure 8.(Molitch, 2017).

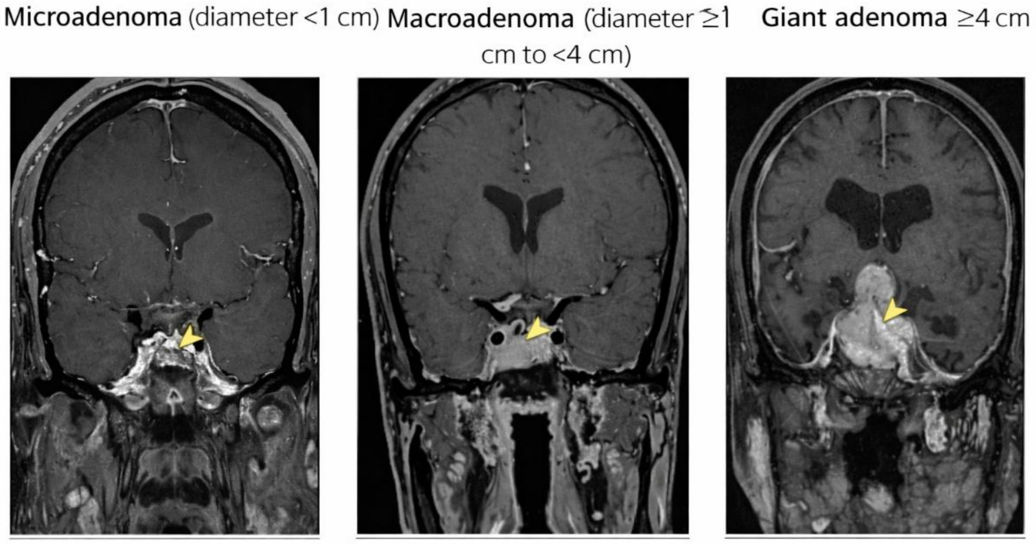

Fig. 8. Magnetic Resonance Imaging gf Pituitary Adenomas(Molitch, 2017).

⇒ Rathke's Cleft Cyst

The cleft cyst Rathke has is a benign, not cancerous, fluid-filled growth that often appears at the base of the brain, between the two lobes of the pituitary gland. (Larkin et al., 2014). When an embryo is developing, Rathke's pouch, a sac-like structure, gives rise to the anterior lobe of the pituitary gland. The cyst is believed to develop when the Rathke pouch's interior does not disappear as it usually does during normal fetal development. This creates a gap that will eventually fill with fluid and expand(Han et al., 2014). Rathke's cleft cyst patients were born with the disorder. Most Rathke's cleft cysts do not exhibit symptoms, so diagnosis is rare. It develops in some individuals, but not others, and why certain cysts cause symptoms is unknown, while others do not. Rathke's cleft cyst treatment is more common in women than in men. In children, Rathke's cleft cyst rarely manifests as symptoms or issues. Most often, Adults who undergo an MRI scan to rule out other medical conditions have other medical conditions discovered (Lu et al., 2020). In Figure 9, the cyst was described as compressing the optic chiasm (29%) (Prokop-Piotrkowska et al., 2018).

Fig. 9. M.R. Image of Rathke Cleft Cyst(Prokop-Piotrkowska et al., 2018).

Based on this type, which is shown in the previous section, many previous works have addressed this topic. Below is a table (1) of the most important works, with an explanation of each research's goal within the table's framework to summarise the previous works. A graph comparing earlier research on brain tumour detection is shown in Figure 10. According to the findings, the initial convolutional neural network (CNN) model had an accuracy of almost 96%. In addition to correctly differentiating between healthy and sick photos, the model was able to catch the majority of diseased instances without missing any, as evidenced by its extremely high sensitivity and near-perfect accuracy. It is therefore a useful model for detecting brain tumours. With an accuracy of roughly 94% and a comparatively lower sensitivity, the second customised CNN model performed marginally worse than the baseline CNN model. This indicates that although the customisation worked well, it was not superior to the baseline network. The accuracy of the third deep CNN model was between 93% and 94%, and while it wasn't the best, the sensitivity was pretty close to the accuracy. This demonstrates that in this case, the network's added depth did not offer a discernible benefit over conventional CNNs. With an accuracy of roughly 92%, the autoencoder model performed worse than any of the earlier models. In comparison to other models, its sensitivity was likewise low. This indicates that even though the autoencoder could extract features from images, it was insufficient to perform optimally on a sensitive task like tumour detection. The accuracy of the MobileNetV2 + SVM model was close to 95–96%, which showed very good results. Additionally, it was highly sensitive and nearly accurate. Combining the strengths of SVM (a reliable classification algorithm) and MobileNetV2 (a lightweight and quick feature extraction algorithm), this model produced results that were extremely competitive, possibly the best of all the approaches discussed. The graph demonstrates that while all models performed exceptionally well (above 90%), the traditional CNNs and MobileNetV2 + SVM models outperformed the others, with an accuracy rate of nearly 96%. The autoencoder performed marginally worse, making it the comparatively weakest. Results from the remaining CNNs (deep CNNs and ad hoc CNNs) were in the middle.

Table 1 - Classifying the MRI Brain Tumours using a Convolutional Neural Network. (Badža & Barjaktarović, 2020).

Year	Dataset	Methods	Aim	Limitation	Result
2020	**figshare** Integrated 10-fold cross-validation scheme with a 60/20/20 data split of training/validation/independent.)	- CNN - Augmentation(90 degrees) - Resizing (256*256)	A designed, low-complexity CNN model that was configured to classify brain tumors into three categories. The model is optimized in T1-weighted CE-MRI and focuses on high efficiency in feature extraction and requires much fewer parameters than conventional pre-trained networks.	• The researcher suggests modifying the structure for brain Surgery, tumour classification and exact location. • Review the results in a limited way, not detail each type of disease and its results, and review the results in general and brief.	**accuracy** 95% **Average Precision** 94.81 Average Recall 95.07 Average F1-Score 94.93

Table 2 - Quick Tumour Net: Rapid Automated Multiclass Brain Tumour Segmentation (Maas et al., 2021).

Year	Dataset	Methods	Aim	Limitation	Result
2021	•Figshare	- CNN	propose an end-to-end approach for brain tumour segmentation, capitalising on a modified version of QuickNAT, a brain tissue type segmentation deep convolutional Neural Network (CNN)	The data set's size, the training volume, and the test were not mentioned.	**accuracy** Meningioma=97 Glioma=84 Pituitary tumor=97 **Mean%** Meningioma=83.3 Glioma=63.5 Pituitary tumor=85.6

Table 3 - Deep CNN for Brain Tumor Classification(Ayadi et al., 2021).

Year	**Dataset**	**Methods**	**Aim**	**Limitation**	**Result**
2021	• Figshare • Radiopaedia Dataset • REMBRANDT Dataset (evaluated using 70% from train fold as training and 30% as validation)	• CNN • Resizing (256×256) • Augmentation • Rotation(5° 90° 135° 180° 225° 270° 315°) • Flip(LEFT_RIGHT TOP_BOTTOM) • Gaussian Blur (Sigma value) • Sharpen (lightness value	Using CNN to solve the classification issue for brain tumors. Proposed a new classifying model for MRI brain cancers that includes multiple layers. Three datasets are used to experimentally assess the suggested model.	The number of epochs is 20, with a batch size of 16 in the proposed system. The process of choosing the optimal epochs was manual; that is, no algorithm was used to stop epochs when there was no change in the results, and this method is the latest compared to the traditional method	Figshare Dataset **accuracy** Meningioma=95.23 Glioma=95.34 Pituitary tumor=98.43 **Sensitivity** Meningioma= 89.68 Glioma= 94.46 Pituitary tumor= 99.03 **Specificity** Meningioma= 96.9 Glioma= 97 Pituitary tumor= 98.17 **Precision** Meningioma= 89.68 Glioma= 96.48 Pituitary tumor= 95.93 **F1-score** Meningioma= 89.68 Glioma= 95.45 Pituitary tumor= 97.45

Table 4 - MRI Image-Based Brain Tumour Segmentation Using Convolutional Autoencoder (Badža & Barjaktarović, 2021).

Year	**Dataset**	**Methods**	**Aim**	**Limitation**	**Result**
2021	Figshare (20% of the data is used for testing, 20% for validation, and 60% for training)	TensorFlow 2.4.0 was used to develop convolutional layers in Google Colaboratory. Moreover, received instruction on a GPU. Tesla P100. • Resizing (256×256) • Augmented(90 degrees)	Introduce a novel convolutional neural autoencoder that uses semantic segmentation to segment brain tumours.	Reviewing the results in a limited way and not detailing each type of disease, what its results are, and reviewing the results in general and briefly	**accuracy.** 99.17 **mean Acc for** augmented **99.4%**

Table 5 - Utilizing deep Neural Network and Multiclass SVM for Multimodal Brain Tumour Identification (Maqsood et al., 2022).

Year	**Dataset**	**Methods**	**Aim**	**Limitation**	**Result**
2022	**•Figshare** ➢ **BraTS 2018**	- NAA(neural network architecture) - MobileNet V2 - SVM - Resizing (256 × 256)	This five-step method is what is suggested. First, the edges in the source image are identified using linear contrast stretching. Step two involved creating unique 17-layer deep brain tumour models divided using a neural network architecture. The third action A modified MobileNetV2 architecture is employed for feature extraction, and transfer learning is used for training. In the fourth step, the optimal feature selection was achieved by combining a multiclass support vector machine (M-SVM) with an entropy-based controlled method. In the last stage, meningioma, glioma, and pituitary images are classified as brain tumours using M-SVM.	-The used dataset contains three diseases and contains details. The results were not reviewed in detail for each disease; the review was conducted in general. - The amount of testing and training for the dataset was not mentioned	**Accuracy** 98.92% **Sensitivity** 98.82% **Specificity** 99.02% **Dice coefficient index** 97.87%

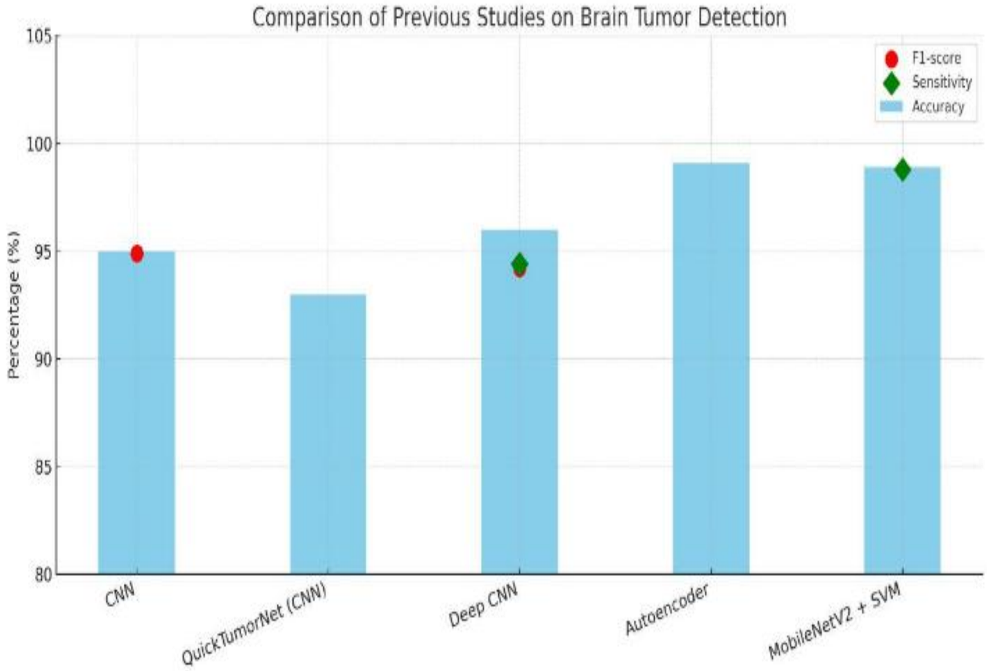

Fig. 10. Illustrates the Differences Between the Studies.

3. Research Methods

Diagnosing tumours is critical given the development of malignant diseases and the speed at which they spread. Therefore, there is still an urgent need for research and development on this topic. Figure 11 shows the proposed system.

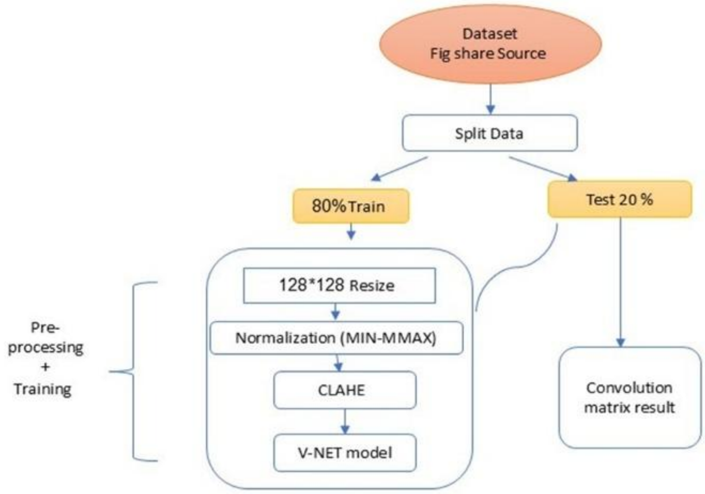

Fig. 11. Proposed System Block Diagram.

3.1 Dataset (Fig share)

This study utilises a publicly accessible benchmark dataset sourced from the Figshare repository. It includes T1-weighted contrast-enhanced magnetic resonance imaging (MRI) scans obtained from Nanfang Hospital and Tianjin Medical University General Hospital in China.

There are 3,064 photos in the dataset, each with a resolution of 512 × 512 pixels. They were taken from 233 patients. There are three forms of brain tumours in it: 1,426 glioma photographs, 708 meningioma images, and 930 pituitary tumour images. The MRI scans were taken from three different anatomical planes: sagittal (1,025 images), axial (994 images), and coronal (1,045 images). This made sure that the spatial views were different. The collection also includes binary tumour masks, where pixel values of 1 indicate tumour areas and 0 indicate background tissue. This makes it easier to learn supervised learning for segmentation problems. It is vital to remember that the number of photos per patient varies, which is how clinical data is usually distributed in the real world. Because this dataset includes so many different tumour types, imaging planes, and patient samples, it is a good way to test how well deep learning models perform at finding and separating brain tumours. Table 6 provides details of the dataset and shows a few MRI images in axial view.

Table 6 - Details of the Fig share dataset(Deepak & Ameer, 2021).

Tumor type	No. of patients	No. of images	Sample image
Meningioma	82	708	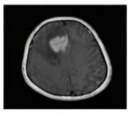
Glioma	89	1426	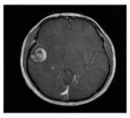
Pituitary tumor	62	930	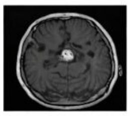

3.3 Preprocessing Stage

The performance of the suggested brain tumour detection and segmentation system is dependent on the quality of the initial data. To streamline the deep learning procedure, I created a multi-step preprocessing pipeline to remove artefacts, standardise input formats, and accentuate subtle pathological structures in the MRI slices. The following paragraphs outline the technical interventions that are included in the proposed framework:

3.1. Data Partitioning

This is the first step where the dataset is partitioned into training and testing subsets systematically. This is used to make sure that the model is optimised on a healthy learning set and at the same time has an independent set of unseen data to test the architectural performance and generalisation abilities.

3.2. Dimensional Standardisation (Resizing)

To match the input size requirements of the V-Net architecture, all MRI slices were resized to a uniform 128x128-pixel dimension. This particular resolution was chosen after trial and error, which showed that a 128x128 scale offers the best trade-off between retaining important spatial information and remaining computationally efficient at the time of training. 3.3. Linear Intensity Normalisation. A Min-Max normalisation technique was used to ensure faster gradient convergence and stabilisation during the learning process. The raw pixel values are normalised to a standard range of [0, 1] by the following expression

$$\mathrm{X\,norm} = \frac{(\mathrm{X} - \mathrm{X\,min})}{(\mathrm{X\,max} - \mathrm{X\,min})}$$

By re-scaling the data according to the specific bit-depth of the images (i.e. 8-bit or 12-bit), the model becomes less sensitive to changes in absolute intensity values, and the loss function is optimised more predictably.

3.4 Adaptive Contrast Enhancement (CLAHE)

One of the fundamental elements of the proposed pipeline is the use of Contrast-Limited Adaptive Histogram Equalisation (CLAHE). In contrast to global equalisation techniques, CLAHE works on localised areas (tiles) and calculates multiple histograms to reassign brightness values. The method is specifically selected because it:

Enhance Local Definition: Refine the border of various brain tissues and tumour margins.

Reduce Noise Amplification: The algorithm mitigates the over-amplification of noise in uniform areas, a typical problem of conventional Adaptive Histogram Equalisation (AHE), by using a pre-defined clip limit.

Enforce Visual Continuity: Bilinear interpolation is used to ensure that the tiles are seamlessly joined together, removing boundary artifacts.The effect of this suggested improvement is evident in Figure 12, which shows that the definition of edges and the differentiation between grey/white matter are much better than in the input.

The quality of the initial data is significant to the efficiency of the proposed brain tumour detection and segmentation system. To streamline the deep learning process, I created a multi-step preprocessing pipeline to remove artefacts, standardise input formats, and enhance subtle pathological features in the MRI slices.

figure 12 visually depicts the effect of this proposed enhancement since the definition of edges and the difference between the gray/white matter are much better than the input itself.

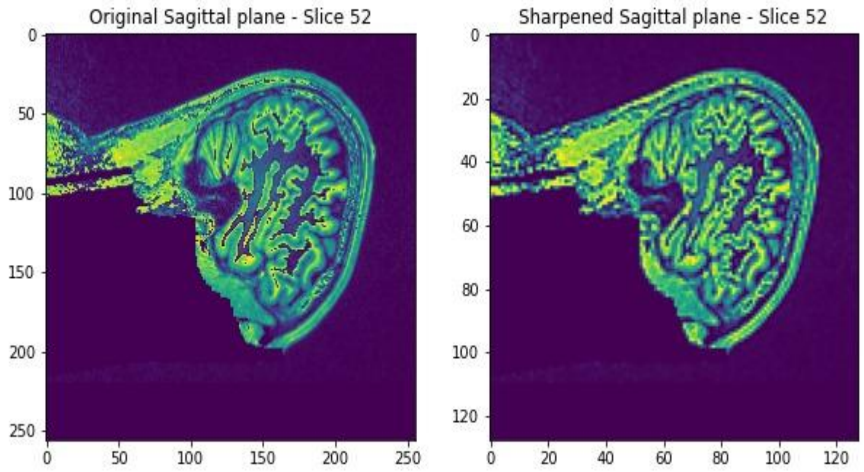

Fig. 12. Steps of Prepressing Stage in Proposed System.

3.5 Training Stage

This study focuses on tumour segmentation and classification. The model learns from data about different types of tumours and different types of data. Instead of just giving a general, clear label, it defines a precise, wide location and voxel-level bounds within MRI images. Figure 13 shows V-Net's architecture, which was used to segment skull tumours.

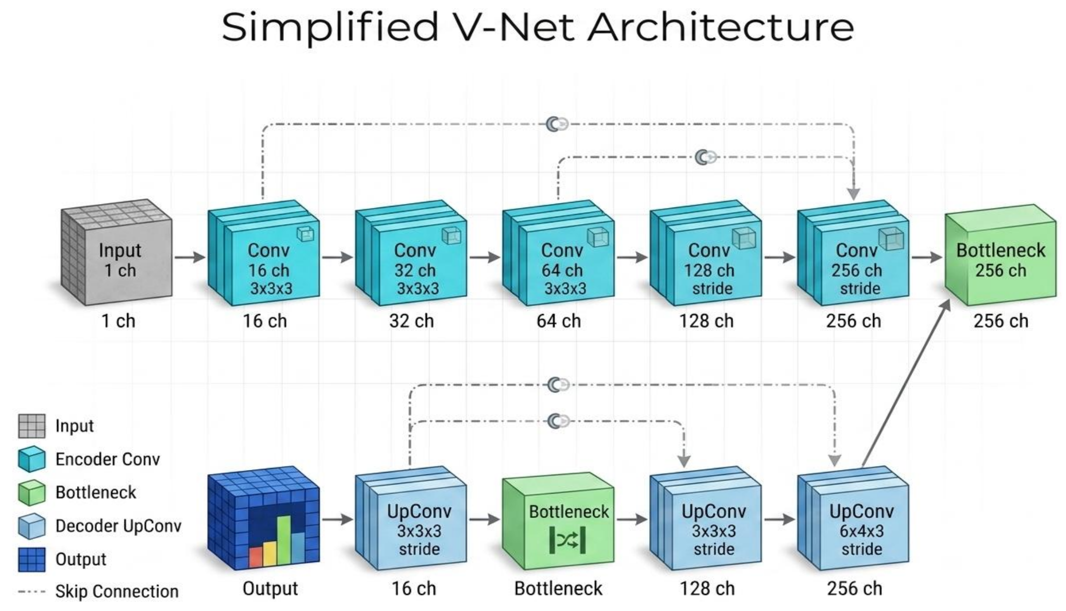

Fig. 13. Illustrates how skull tumours were segmented using V-Net's Design.

A 3D V-Net framework was used to separate tumours. This framework is built on an encoder-decoder structure. The encoder uses pre-defined 3D fills to get general data, while the decoder uses those fills to build the segment map and get Direct details. To enable extensive boundary analysis, skip connections were used to route exact operational data from the encoder stages to the advanced decoder stages. At bottlenecks, the data is shown in the most abstract way possible. Finally, a new comfort compressor (SoftMax or Sigmoid) is used to identify potential voxel-level separators between distinct regions. This type of biological dataset is well-suited to V-Net because it handles three-dimensional (3D) data. It lets you separate contextual information between different parts of the brain. This is essential since these parts often have different shapes and structures.

Also, the use of a dice-loss function addresses the data imbalance between small and tissue areas quite well. This also means that the proposed model only needs to divide the different types of regions into segments and assign each segment a unique type.

The following summary, V-Net Architecture for Skull Tumour Segmentation-Net, is a three-dimensional fully convolutional neural network designed specifically for volumetric medical image segmentation. Its architecture follows an encoder–decoder paradigm shaped like the letter "V", where the encoder path gradually extracts deep features through strided 3D convolutions and residual blocks. In contrast, the decoder path reconstructs the segmentation map using transposed convolutions and symmetric skip connections. The residual blocks stabilise training of very deep layers, whereas the skip connections ensure that fine-grained spatial details lost during down-sampling are preserved during up-sampling. The final layer applies a convolution followed by a SoftMax (or sigmoid) activation to generate a voxel-wise probability map.

For brain and skull analysis, V-Net is particularly effective because it operates directly on 3D MRI or CT volumes, capturing contextual information across slices. This volumetric representation is critical for detecting irregular tissue growths, such as brain or skull tumours, which often extend across multiple slices and vary in size and shape. By leveraging the Dice loss function, V-Net addresses the severe class imbalance between small tumour regions and the much larger healthy tissue, thereby improving sensitivity to tumour boundaries.

In tumour detection within the skull, V-Net enhances clinical workflows by:

1. Accurate delineation of tumour boundaries, which is essential for pre-surgical planning and radiotherapy.
2. Robust handling of variability in tumour size, intensity, and location across patients.
3. Automation of a previously manual and time-consuming segmentation process, reducing inter-observer variability.

Overall, V-Net provides a powerful backbone for automated brain and skull tumour segmentation, demonstrating significant improvements over conventional 2D CNNs by exploiting 3D spatial context and residual learning.

After applying the V-Net model to segment the tumour, the resulting voxel-level probability map is utilised to determine whether there is a tumour. The segmentation mask is looked at. If the map has areas with positive values (which means there is a tumour), the image is called tumorous. If no cancerous spots are found, the situation is considered benign. So, an independent model doesn't directly determine the classification (tumour/non-tumour); instead, it uses the segmentation results to infer the classification, thereby linking tumour location to diagnostic decision-making. This method makes the results more reliable because the final choice is based on precise spatial information rather than on a broad image classification.

4. Results and Discussion

The performance of the proposed system was evaluated using both segmentation and classification metrics to obtain a comprehensive performance analysis. For the tumour segmentation task, the Dice coefficient and the Intersecting Union (IoU) metric were used to measure the degree of correspondence between the predicted areas of the model and the actual data (ground truth). The Dice coefficient is defined as follows:

$$\mathbf{Dice = (2 \times |A \cap B|) / (|A| + |B|)}$$

reas. The results shown in Table 7 indicate that the proposed V-Net model achieved a Dice value of 99.9% on the test data, demonstrating high accuracy in identifying tumour boundaries.

Table 7: Recap of the suggested system's results. The percentage of overlap between the target mask and the predicted output can be estimated using the Intersection over Union (IoU) metric.

'

Table 7-Results of The Proposed System

Metrics	Accuracy	F1	Dice-score
Training	98.6%	98%	null
Testing	99.1%	99%	99.9%

The Intersection over Union (IoU) measure assesses the overlap between the target mask and the expected output. Figure 14 shows (a) Ground truth: This image represents the exact, manually segmented, or true representation of the brain region of interest (most likely white matter or grey matter). It serves as a reference for evaluating the segmentation algorithm's performance. (b) Predicted: This image depicts the segmentation of the same brain region. (c) \(a\cup b\): This image represents the union of the ground truth (a) and the predicted segmentation (b). It highlights all pixels present in either the ground truth or the predicted segmentation, or in both. This indicates the total area covered by both the true and predicted segmentations. (d) \(a\cup b\): This image represents the intersection of the ground truth (a) and the predicted segmentation (b). This system only highlights pixels shared by the ground truth and the predicted segmentation, indicating that the accurately segmented region overlaps with the true region.

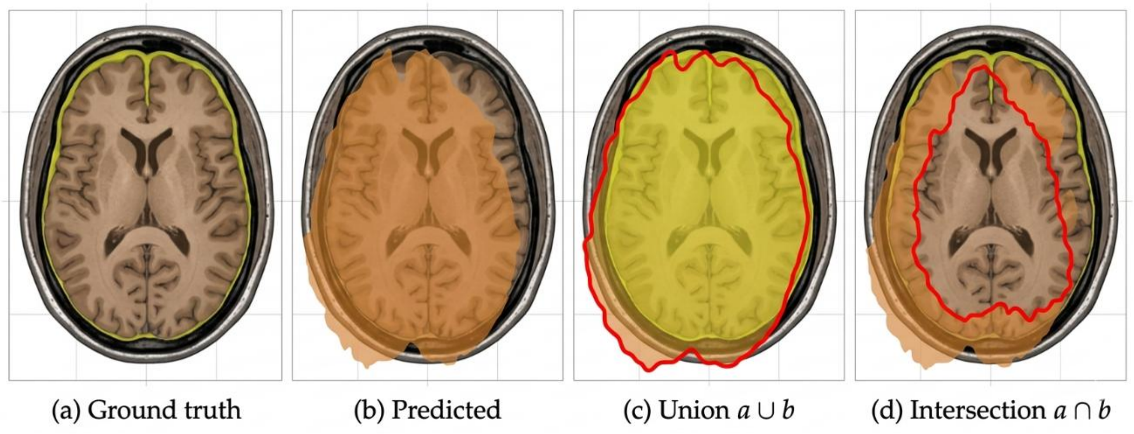
(a) Ground truth (b) Predicted (c) Union $a \cup b$ (d) Intersection $a \cap b$

Fig. 14. Demonstrates the Concept of Ground Truth and Predicted Segmentation, It Also Illustrates the Specific Union and Intersection Processes Between These Segmentations.

Furthermore, a binary classification task (infected/uninfected) was derived based on the segmentation results. If the segmentation map showed a tumour area, the image was classified as “infected,” and if no tumour area was found, it was classified as “uninfected.” Regarding classification, accuracy and F1 scores were used to evaluate performance. The model achieved 99.1% accuracy and a 99% F1 score on the test data. The data was divided into 80% for training and 20% for testing. Early Stopping was employed to prevent overlearning, with training stopped at Epoch 21.

The following summarises the metrics used to evaluate the training of the proposed approaches:

1. Loss: an approach for assessing the precision of an algorithm's dataset modelling is the loss function. It depends mathematically on deep learning and the parameters of the machine learning algorithm.
2. F1-Score: The harmonic mean of accuracy and recall is denoted as F1.
3. Accuracy: Accuracy is how closely an expression or measurement matches an actual value. Some fields, like science, define it more precisely.

However, the model shows average F1 Scores of 98.2% and a validation F1 score of 97.8%. Since there was no progress in the F1-scores validation for the next 10 iterations (as determined by the patience parameter), the number of epochs ends at epoch 21 due to the Early halting function. Figure 15: A confusion matrix is a summary of the performance of a classification model. It is used to illustrate an algorithm's performance by displaying the number of correct and incorrect predictions for each class.

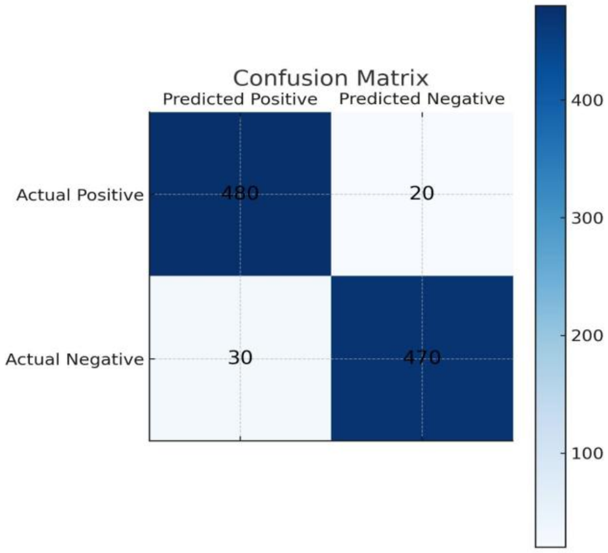

Fig. 15. A Confusion Matrix

Table 8 shows the values extracted from the confusion matrix, which indicates the classifier's performance by the number of cases classified correctly or incorrectly. The results are divided into four categories: True Positive, True Negative, False Positive, and False Negative.

Table 8- Basic Classification Performance Metrics.

Four outcomes of a classifier	Tree Positive	False Negative	False Positive	True Negative
Total images count	480	20	30	470

A bar chart, Figure 16, entitled, "Performance Metrics (Estimated Example), indicates the estimated performance of the model with different classification metrics. The highest measure is precision (96.0%), which means that the percentage of correct identification of positive cases is high among all the predicted positive cases. Specificity (95.9%), Accuracy (95.0%), F1-score (95.0%), and Dice (95.0%) also show strong performance. Recall (Sensitivity) (94.1) is a little below other measures indicating the capacity of the model to find all the real positive cases.

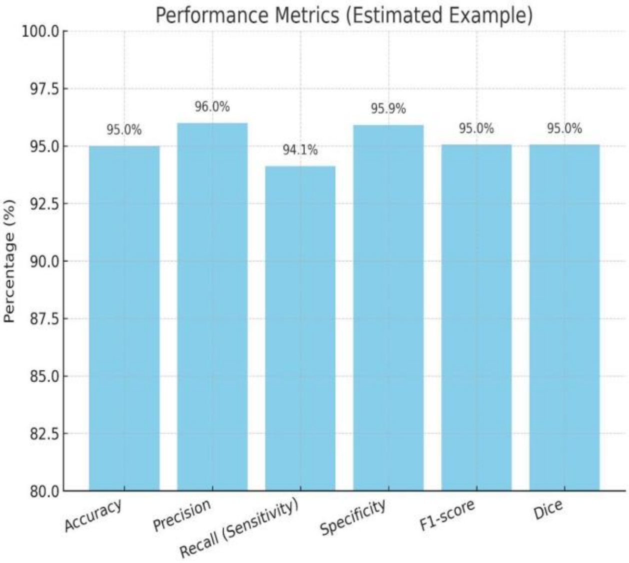

Fig. 16. Show Bar Chart for Performance Metrics. It Displays Values (Accuracy, Precision, Recall, Specificity, F1-Score, Dice) As Percentages.

5. Conclusion

This paper discussed the design and creation of a system to segment brain tumours based on magnetic resonance imaging (MRI) images, using a three-dimensional V-Net architecture, which is based on deep learning. We used a number of different quantitative criteria to see how well the model worked. The segmentation job achieved a DICE score of 99.9% and a classification accuracy of 99.1% (affected/unaffected) and F1 of 99%. This demonstrates that the model is rather effective in detecting tumours and diagnosis. Although these are good results, there are a number of issues with the model. It was tested on a given data, which might lessen its applicability to other kinds of medical data. Moreover, the model is based on a single type of MRI imaging which might not work well in more complex cases. This approach can be improved in the future by using hybrid models that mix convolutional neural networks (CNNs) and transformer models to take advantage of both short- and long-range associations. Multimodal MRI information can also be used to locate tumours more precisely. And, to ensure that this system is stable and precise to assist doctors in making decisions, it must be tested on real-world data of multiple hospitals and reviewed by knowledgeable doctors. The proposed solution has shown good results, but more study and experiment are required to enhance its feasibility in the field of medicine.

References

Alahmari, A. (2020). *Acoustic neuroma: A case series*. *1*, 1–6.

Arabahmadi, M., Farahbakhsh, R., & Rezazadeh, J. (2022). Deep learning for smart Healthcare—A survey on brain tumour detection from medical imaging. *Sensors*, *22*(5), 1960.

Arokia Jesu Prabhu, L., & Jayachandran, A. (2018). Mixture model segmentation system for parasagittal meningioma brain tumour classification based on a hybrid feature vector. *Journal of Medical Systems*, *42*, 1–6. https://doi.org/10.1007/s10916-018-1094-3

Arvanitis, C. D., Ferraro, G. B., & Jain, R. K. (2020). The blood–brain barrier and blood–tumour barrier in brain tumours and metastases. *Nature Reviews Cancer*, *20*(1), 26–41. https://doi.org/10.1038/s41568-019-0205-x

Ayadi, W., Elhamzi, W., Charfi, I., & Atri, M. (2021). Deep CNN for brain tumour classification. *Neural Processing Letters*, *53*, 671–700. https://doi.org/10.1007/s11063-020-10398-2

Badža, M. M., & Barjaktarović, M. Č. (2020). Classification of brain tumours from MRI images using a convolutional neural network. *Applied Sciences*, *10*(6), 1999. https://doi.org/10.3390/app10061999

Badža, M. M., & Barjaktarović, M. Č. (2021). Segmentation of brain tumours from MRI images using a convolutional autoencoder. *Applied Sciences, 11*(9), 4317. https://doi.org/10.3390/app11094317

Cabezas-Camarero, S., & Pérez-Segura, P. (2022). Liquid biopsy in head and neck cancer: Current evidence and future perspective on squamous cell, salivary gland, paranasal sinus and nasopharyngeal cancers. *Cancers, 14*(12), 2858. https://doi.org/10.3390/cancers14122858

Chahal, P. K., Pandey, S., & Goel, S. (2020). A survey on brain tumor detection techniques for MR images. *Multimedia Tools and Applications*, *79*, 21771–21814. https://doi.org/10.1007/s11042-020-08898-3

Chen, B., Zhang, L., Chen, H., Liang, K., & Chen, X. (2021). A novel extended Kalman filter with support vector machine based method for the automatic diagnosis and segmentation of brain tumors. *Computer Methods and Programs in Biomedicine, 200,* 105797. https://doi.org/10.1016/j.cmpb.2020.105797

Chen, X., Tong, Y., Shi, Z., Chen, H., Yang, Z., Wang, Y., Chen, L., & Yu, J. (2019). Noninvasive molecular diagnosis of craniopharyngioma with MRI-based radiomics approach. *BMC Neurology, 19*, 1–11. https://doi.org/10.1186/s12883-018-1216-z

David, D. S. (2019). Parasagittal meningioma brain tumor classification system based on MRI images and multi phase level set formulation. *Biomedical and Pharmacology Journal, 12*(2), 939–946. https://doi.org/10.13005/bpj/1720

Deckers, C., Steyvers, M. J., Hannink, G., Schreuder, H. W. B., De Rooy, J. W. J., & Van Der Geest, I. C. M. (2020). Can MRI differentiate between atypical cartilaginous tumors and high-grade chondrosarcoma? A systematic review. *Acta Orthopaedica*, *91*(4), 471–478. https://doi.org/10.1080/17453674.2020.1763717

Deepak, S., & Ameer, P. M. (2021). Automated categorization of brain tumor from mri using cnn features and svm. *Journal of Ambient Intelligence and Humanized Computing*, *12*, 8357–8369. https://doi.org/10.1007/s12652-020-02568-w

Ferrari, M., Taboni, S., Carobbio, A. L. C., Emanuelli, E., Maroldi, R., Schreiber, A., Mattavelli, D., Farina, D., Nicolai, P., & Battaglia, P. (2021). Sinonasal squamous cell carcinoma: A narrative reappraisal of the current evidence. *Cancers, 13*(11), 2835. https://doi.org/10.3390/cancers13112835

Gazendam, A., Popovic, S., Parasu, N., & Ghert, M. (2023). Chondrosarcoma: A Clinical Review. *Journal of Clinical Medicine*, *12*(7), 2506. https://doi.org/10.3390/jcm12072506

Gelderblom, H., Hogendoorn, P. C. W., Dijkstra, S. D., Van Rijswijk, C. S., Krol, A. D., Taminiau, A. H. M., & Bovee, J. V. M. G. (2008). The clinical approach towards chondrosarcoma. *The Oncologist, 13*(3), 320–329. https://doi.org/10.1634/theoncologist.2007-0237

Georgiadis, P., Kostopoulos, S., Cavouras, D., Glotsos, D., Kalatzis, I., Sifaki, K., Malamas, M., Solomou, E., & Nikiforidis, G. (2011). Quantitative combination of volumetric MR imaging and MR spectroscopy data for the discrimination of meningiomas from metastatic brain tumors by means of pattern recognition. *Magnetic Resonance Imaging*, *29*(4), 525–535. https://doi.org/10.1016/j.mri.2010.11.006

Gordillo, N., Montseny, E., & Sobrevilla, P. (2013). State of the art survey on MRI brain tumor segmentation. *Magnetic Resonance Imaging, 31*(8), 1426–1438. https://doi.org/10.1016/j.mri.2013.05.002

Han, S. J., Rolston, J. D., Jahangiri, A., & Aghi, M. K. (2014). Rathke's cleft cysts: review of natural history and surgical outcomes. *Journal of Neuro-Oncology, 117,* 197–203. https://doi.org/10.1007/s11060-013-1272-6

Harris, J. C., Eide, J. G., Kshirsagar, R. S., Brant, J. A., Palmer, J. N., & Adappa, N. D. (2022). Carcinosarcoma of the nasal cavity and paranasal sinuses: Review of the national cancer database. *World Journal of Otorhinolaryngology - Head and Neck Surgery*, *9*(02), 115–122. https://doi.org/10.1002/wjo2.82

Hashemzehi, R., Mahdavi, S. J. S., Kheirabadi, M., & Kamel, S. R. (2020). Detection of brain tumors from MRI images base on deep learning using hybrid model CNN and NADE.

Biocybernetics and Biomedical Engineering, *40*(3), 1225–1232. https://doi.org/10.1016/j.bbe.2020.06.001

Hu, A., & Razmjooy, N. (2021). Brain tumor diagnosis based on metaheuristics and deep learning. *International Journal of Imaging Systems and Technology*, *31*(2), 657–669. https://doi.org/10.1002/ima.22495

Jia, Z., & Chen, D. (2020). Brain tumor identification and classification of MRI images using deep learning techniques. *IEEE Access*, *8*, 195649–195666. https://doi.org/10.1109/ACCESS.2020.3016319

Lake, M. G., Krook, L. S., & Cruz, S. V. (2013). Pituitary adenomas: an overview. *American Family Physician*, *88*(5), 319–327.

Larkin, S., Karavitaki, N., & Ansorge, O. (2014). Rathke's cleft cyst. *Handbook of Clinical Neurology*, *124*, 255–269. https://doi.org/10.1016/B978-0-444-59602-4.00017-4

Lu, V. M., Ravindran, K., Perry, A., Graffeo, C. S., Dawood, H. Y., Van Gompel, J. J., Mekary, R. A., & Smith, T. R. (2020). Recurrence of Rathke's cleft cysts based on gross total resection of cyst wall: a meta-analysis. *Neurosurgical Review*, *43*, 957–966. https://doi.org/10.1007/s10143-019-01107-2

Maas, B., Zabeh, E., & Arabshahi, S. (2021). QuickTumorNet: fast automatic multi-class segmentation of brain tumors. *2021 10th International IEEE/EMBS Conference on Neural Engineering (NER)*, 81–85. https://doi.org/10.1109/NER49283.2021.9441286

Maqsood, S., Damaševičius, R., & Maskeliūnas, R. (2022). Multi-modal brain tumor detection using deep neural network and multiclass SVM. *Medicina*, *58*(8), 1090. https://doi.org/10.3390/medicina58081090

Mark, I. T., Van Gompel, J. J., Inwards, C. Y., Ball, M. K., Morris, J. M., & Carr, C. M. (2022). MRI enhancement patterns in 28 cases of clival chordomas. *Journal of Clinical Neuroscience*, *99*, 117–122. https://doi.org/10.1016/j.jocn.2022.02.037

Molitch, M. E. (2017). Diagnosis and treatment of pituitary adenomas: a review. *Jama*, *317*(5), 516–524. https://doi.org/10.1001/jama.2016.19699

Mostafa, A. M., El-Meligy, M. A., Alkhayyal, M. A., Alnuaim, A., & Sharaf, M. (2023). A framework for brain tumor detection based on segmentation and features fusion using MRI images. *Brain Research*, *1806*, 148300. https://doi.org/10.1016/j.brainres.2023.148300

Neugut, A. I., Sackstein, P., Hillyer, G. C., Jacobson, J. S., Bruce, J., Lassman, A. B., & Stieg, P. A. (2019). Magnetic resonance imaging-based screening for asymptomatic brain tumors: a review. *The Oncologist*, *24*(3), 375–384. https://doi.org/10.1634/theoncologist.2018-0177

Prokop-Piotrkowska, M., Moszczyńska, E., Daszkiewicz, P., Roszkowski, M., & Szalecki, M. (2018). Symptomatic Rathke cleft cyst in paediatric patients–clinical presentations, surgical treatment and postoperative outcomes–an analysis of 38 cases. *Journal of Pediatric Endocrinology and Metabolism*, *31*(8), 903–910. https://doi.org/10.1515/jpem-2017-0540

Rane, M. (2023). Multimodal Convolutional Neural Network Models Allow for the Accurate Classification and Grading of Preoperative Meningioma Brain Tumors. *MedRxiv*, 2003–2023. https://doi.org/10.1101/2023.03.15.23287326

Raverot, G., & Ilie, M. D. (2022). Immunotherapy in pituitary carcinomas and aggressive pituitary tumors. *Best Practice & Research Clinical Endocrinology & Metabolism*, *36*(6), 101712. https://doi.org/10.1016/j.beem.2022.101712

Sampson, J. H., Gunn, M. D., Fecci, P. E., & Ashley, D. M. (2020). Brain immunology and immunotherapy in brain tumours. *Nature Reviews Cancer*, *20*(1), 12–25. https://doi.org/10.1038/s41568-019-0224-7

Sanjay, V., & Swarnalatha, P. (2022). A survey on various machine learning techniques for an efficient brain tumor detection from MRI images. *IJEER*, *10*(2), 177–182. https://doi.org/10.37391/ijeer.100222

Shimony, N., Gonen, L., Shofty, B., Abergel, A., Fliss, D. M., & Margalit, N. (2017). Surgical resection of skull-base chordomas: experience in case selection for surgical approach according to anatomical compartments and review of the literature. *Acta Neurochirurgica*, *159*, 1835–1845. https://doi.org/10.1007/s00701-016-3032-9

Singh, A. (2016). Review of brain tumor detection from MRI images. *2016 3rd International Conference on Computing for Sustainable Global Development (INDIACom)*, 3997–4000.

Soomro, T. A., Zheng, L., Afifi, A. J., Ali, A., Soomro, S., Yin, M., & Gao, J. (2022). Image segmentation for MR brain tumor detection using machine learning: A Review. *IEEE Reviews in Biomedical Engineering*. https://doi.org/10.1109/RBME.2022.3185292

Taylor, M. A., & Saba, N. F. (2021). Cancer of the paranasal sinuses. *Hematology/Oncology Clinics*, *35*(5), 949–962. https://doi.org/10.1016/j.hoc.2021.05.006

Tchoketch Kebir, S., Mekaoui, S., & Bouhedda, M. (2019). A fully automatic methodology for MRI brain tumour detection and segmentation. *The Imaging Science Journal*, *67*(1), 42–62. https://doi.org/10.1080/13682199.2018.1545412

Tiwari, A., Srivastava, S., & Pant, M. (2020). Brain tumor segmentation and classification from magnetic resonance images: Review of selected methods from 2014 to 2019. *Pattern Recognition Letters*, *131*, 244–260. https://doi.org/10.1016/j.patrec.2019.11.020

Tosaka, M., Fukasawa, Y., Takahashi, A., Sasaki, A., & Saito, N. (2005). Incidentally detected parafalcine chondrosarcoma. *Acta Neurochirurgica*, *147*, 795–799. https://doi.org/10.1007/s00701-005-0530-6

Zhang, Y., Chen, C., Tian, Z., & Xu, J. (2020). Discrimination between pituitary adenoma and craniopharyngioma using MRI-based image features and texture features. *Japanese Journal of Radiology*, *38*, 1125–1134. https://doi.org/10.1007/s11604-020-01021-4